



**HAL**  
open science

## New Insights into the State Trapping of UV-Excited 2 Thymine 3

Ljiljana Stojanović, Shuming Bai, Jayashree Nagesh, Artur F Izmaylov,  
Rachel Crespo-Otero, Hans Lischka, Mario Barbatti

► **To cite this version:**

Ljiljana Stojanović, Shuming Bai, Jayashree Nagesh, Artur F Izmaylov, Rachel Crespo-Otero, et al..  
New Insights into the State Trapping of UV-Excited 2 Thymine 3. *Molecules*, 2016, 21 (11), pp.1603.  
10.3390/molecules21111603 . hal-02288823

**HAL Id: hal-02288823**

**<https://amu.hal.science/hal-02288823>**

Submitted on 16 Sep 2019

**HAL** is a multi-disciplinary open access archive for the deposit and dissemination of scientific research documents, whether they are published or not. The documents may come from teaching and research institutions in France or abroad, or from public or private research centers.

L'archive ouverte pluridisciplinaire **HAL**, est destinée au dépôt et à la diffusion de documents scientifiques de niveau recherche, publiés ou non, émanant des établissements d'enseignement et de recherche français ou étrangers, des laboratoires publics ou privés.



Distributed under a Creative Commons Attribution 4.0 International License

1 Article

# 2 New Insights into the State Trapping of UV-Excited 3 Thymine

4 Ljiljana Stojanovic <sup>1</sup>, Shuming Bai <sup>1</sup>, Jayashree Nagesh <sup>2</sup>, Artur F. Izmaylov <sup>2,3</sup>, Rachel Crespo-  
5 Otero <sup>4</sup>, Hans Lischka <sup>5,6</sup>, Mario Barbatti <sup>1,\*</sup>

6 <sup>1</sup> Aix Marseille Univ, CNRS, ICR, Marseille, France

7 <sup>2</sup> Chemical Physics Theory Group, Department of Chemistry, University of Toronto, Toronto, ON M5S 3H6,  
8 Canada

9 <sup>3</sup> Department of Physical and Environmental Sciences, University of Toronto Scarborough, Toronto, ON  
10 M1C 1A4, Canada

11 <sup>4</sup> School of Biological and Chemical Sciences, Queen Mary University of London, Mile End Road, London E1  
12 4NS, United Kingdom

13 <sup>5</sup> School of Pharmaceutical Sciences and Technology, Tianjin University, Tianjin, 300072 P. R. China

14 <sup>6</sup> Department of Chemistry and Biochemistry, Texas Tech University, Lubbock Texas 79409, USA

15 \* Correspondence: mario.barbatti@univ-amu.fr; Tel.: +33(0)4 84 52 92 00

16 Academic Editor: Carlos Crespo-Hernandez

17 Received: date; Accepted: date; Published: date

18 **Abstract:** After UV excitation, gas phase thymine returns to ground state in 5 to 7 ps, showing  
19 multiple time constants. There is no consensus on the assignment of these processes, with a dispute  
20 between models claiming that thymine is trapped either in the first ( $S_1$ ) or in the second ( $S_2$ ) excited  
21 states. In the present study, nonadiabatic dynamics simulation of thymine is performed on the basis  
22 of ADC(2) surfaces, to understand the role of dynamic electron correlation on the deactivation  
23 pathways. The results show that trapping in  $S_2$  is strongly reduced in comparison to previous  
24 simulations considering only non-dynamic electron correlation on CASSCF surfaces. The reason for  
25 the difference is traced back to the energetic cost for formation of a CO  $\pi$  bond in  $S_2$ .

26 **Keywords:** Computational theoretical chemistry; Photochemistry; Nonadiabatic dynamics;  
27 Ultrafast processes; Surface hopping; Nucleobases; Thymine.

## 29 1. Introduction

30 After UV excitation, gas phase thymine is back to the ground state within 5 to 7 ps [1]. In the  
31 fourteen years since ultrafast time-resolved spectroscopy of this molecule was reported by the first  
32 time [2], this seems to be the only consensus on the interpretation of its photophysics. The elusive  
33 nature of thymine's photophysics stems from the difficulty of assigning multiple time constants  
34 underlying its time-resolved photoelectron spectrum [1-10]. In fact, a literature survey (see Table 1)  
35 reveals that there is no full agreement on even how many time constants are implicit in those spectra  
36 [1,3,7]. Most of results tend to converge to a three time-constants scheme, with a short sub-picosecond  
37 time constant of about 100-200 fs, a picosecond time constant of about 6 ps, and a nanosecond time  
38 constant, reaching near 300 ns.

39 Taking the picosecond time constant as an indication of internal conversion to the ground state—  
40 which is the most common interpretation—leaves thymine with the longest excited state lifetime  
41 among the isolated nucleobases [7,11]. This fact is on itself puzzling, as thymine's potential energy  
42 surfaces obtained from high-level computational simulations are very similar to those of other short-  
43 lived pyrimidines (uracil, for instance), to justify the time constant differences [12].

44 Computational simulations have revealed that thymine internal conversion after UV excitation  
45 should involve two singlet excited adiabatic states,  $S_1$  and  $S_2$  [12,13]. These states may have  $n\pi^*$  or

46 diverse  $\pi\pi^*$  characters along the reaction paths. There is an extended accessible crossing seam region  
 47 between  $S_2$  and  $S_1$  ( $\pi\pi^*/n\pi^*$ ) [14], as well as between  $S_1$  and the ground state ( $\pi\pi^*/S_0$  and  $n\pi^*/S_0$ ) [15].  
 48 A long-lived triplet  $\pi\pi^*$  state plays a role over longer scales [1,9,16,17] not explored here.

49 In earlier works, thymine's shortest time constant has been assigned to direct internal conversion  
 50 to ground state along a  $\pi\pi^*$  pathway. Such a model—we will refer to it as the “fast  $\pi\pi^*$  model”—was  
 51 proposed on the basis of either analyses of ab initio potential energy surfaces [18,19] or surface  
 52 hopping dynamics on semi-empirical surfaces [20]. Nevertheless, the agreement between these works  
 53 is restricted to this sub-picosecond step: while ref. [18] proposes that the picosecond step would occur  
 54 due to a retarded  $\pi\pi^*$  deactivation, ref. [19] attributes this longer step to a sequential  $\pi\pi^* \rightarrow n\pi^* \rightarrow S_0$   
 55 conversion. Ref. [20], on its turn, also predicts a sequential  $\pi\pi^* \rightarrow n\pi^* \rightarrow S_0$  conversion process, but  
 56 occurring in the sub-picosecond scale.

57 **Table 1.** Excited-state time constants of thymine in the gas phase according to the experiments  
 58 under diverse pump and probe conditions.

Pump (nm)	Probe (nm)	$\tau_1$ (fs)	$\tau_2$ (ps)	$\tau_3$ (ps)	$\tau_4$ (ns)	Ref.
250	200	<50	0.49	6.4		[3]
260	295	175		6.13	>1	[1]
266	2.19 (X-ray)	200-300				[4]
266	400 / 800	<100		7	long	[5]
266	800	200		7		[6]
267	2×400	105		5.12		[7]
267	800	100		7	>1	[8]
267	800			6.4	>100	[2]
270	193				293	[9]
272	800	130		6.5		[10]

59 A different photophysical model was proposed in ref. [13] and later corroborated by ref. [15], both on  
 60 the basis of analysis of ab initio potential energy surfaces. This model—the “ $S_1$  trapping model”—assigns the  
 61 short time constant to a fast  $S_2(\pi\pi^*) \rightarrow S_1(n\pi^*)$  transition, while the picosecond time constant is assigned to  
 62 a  $S_1(n\pi^*) \rightarrow S_0$  transition. Thus, according to this interpretation, the elongated picosecond time constant of  
 63 thymine would be caused by a trapping in the  $S_1$  state.  
 64

65 The  $S_1$  trapping model has been popular among experimentalists, as it apparently correlates well  
 66 with the electron binding energy ( $E_b$ ) observed in time-resolved experiments [1,6,21]. Their argument  
 67 goes as follows: the first ionization potential (IP) of thymine is a  $\pi$  hole, while the second is an n hole.  
 68 Thus, spectral signals at low  $E_b$  near the first IP should be caused by probing the  $\pi\pi^*$  state, while  
 69 spectral signals at large  $E_b$  near the second IP should be caused by probing the  $n\pi^*$  state. Because the  
 70 signal in the picosecond scale comes from large  $E_b$ , this would be an evidence that thymine is in the  
 71  $n\pi^*$  state during the picosecond regime. The problem with this argument is that it assumes that  
 72 electrons are usually ejected with the maximum electron kinetic energy (or minimum  $E_b$ , near the IP).  
 73 This is correct only for ionization of stationary states. When probing wave packets, a much wider  
 74 range of electron kinetic energies should be expected [22]. Thus, while it is true that spectral signal  
 75 near the first IP should be essentially due to  $\pi\pi^*$  probing, the signal near the second IP contains not  
 76 only information from the  $n\pi^*$  probing, but also information from  $\pi\pi^*$  probing of electrons being  
 77 ejected with low kinetic energy.

78 Although this analysis of the electron kinetic energy does not disprove the  $S_1$  trapping model  
 79 (which is good for us, as will be advocating for it later), it at least reduces its strength. And if that  
 80 were not enough, there is still a third model for thymine deactivation in direct competition with it, the  
 81 “ $S_2$  trapping model.”

82 The  $S_2$  trapping was first proposed on the basis of multiple spawning dynamics on CASSCF  
 83 surfaces [23]. These simulations, limited to a short sub-picosecond time scale, showed that after  
 84 excitation into  $S_2(\pi\pi^*)$  state, conversion to  $S_1(n\pi^*)$  was unexpectedly slow. This led to the hypothesis  
 85 that the picosecond time constant was due to thymine's trapping in  $S_2$ , while the short sub-picosecond

86 time constant was caused by relaxation of the  $\pi\pi^*$  state between the Franck-Condon region and the  
 87  $S_2$  minimum.

88 The  $S_2$  trapping model got some additional support from surface hopping dynamics still on  
 89 CASSCF surfaces [14,24]. These simulations were performed on longer time scales than in the original  
 90 multiple spawning simulations and confirmed that slow  $S_2 \rightarrow S_1$  transfer. However, the surface  
 91 hopping results also added a new layer of complexity, as they showed that the  $S_2$  trapping could only  
 92 explain a retard of about 2 ps in the lifetime; therefore, to reach a 6 ps time constant, thymine should  
 93 also be trapped in  $S_1$  after the  $S_2 \rightarrow S_1$  transition. A final bit of complexity was later steered into the  
 94 model by wave packet dynamics [25]. It showed that even the common hypothesis that only the  $\pi\pi^*$   
 95 state is excited needs to be relaxed, as vibronic couplings could lead to a substantial  $n\pi^*$  population  
 96 within the first 50 fs of dynamics, with the remaining  $\pi\pi^*$  population trapped in a flat  $S_2$ . Thus,  
 97 together, these results from surface hopping and wave packet dynamics seemed to point out to a new  
 98 “ $S_2$  and  $S_1$  trapping model”.

99 A couple of years ago, however, the  $S_2$  trapping hypothesis was challenged by time-resolved  
 100 Auger spectroscopy [4], which combined with spectrum simulations at CIS level made a good case  
 101 towards a population transfer to  $n\pi^*$  state within 200-300 fs. Once more, the  $S_1$  trapping model would  
 102 be invoked to explain the picosecond time constant.

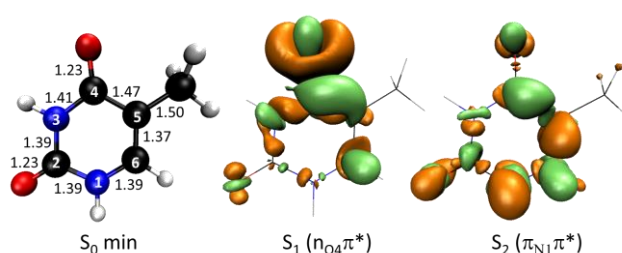
103 Giving this cloudy state of affairs, we decided to revisit thymine dynamics. Although multiple  
 104 spawning and surface hopping dynamics have provided some compelling arguments for the  $S_2$   
 105 trapping, these simulations have a common major weak point: they were based on CASSCF surfaces.  
 106 CASSCF does an excellent job recovering non-dynamic electron correlation near intersections  
 107 between the *ground and the first excited states*, however, it neglects most of dynamic electron  
 108 correlation, which is present through the whole reaction path. And this poses a serious problem: the  
 109 key step to determine the occurrence (or not) of the  $S_2$  trapping is the  $S_2$  dynamics up to the  $S_2/S_1$   
 110 crossing. On this region of the potential energy surface, we do not expect any relevant impact of non-  
 111 dynamic electron correlation, but we are sure that dynamic electron correlation plays a role; for  
 112 instance, correcting the strong overestimation of the  $\pi\pi^*$  energy typical of CASSCF predictions  
 113 [15,19]. Therefore, we have approached the problem through surface hopping simulations based on  
 114 ADC(2) method, which, quite opposite to CASSCF, recovers well dynamic correlation, but neglects  
 115 non-dynamic correlation. We can already anticipate that this methodological change had a major  
 116 impact on the results: the  $S_2$  trapping is strongly reduced.

## 117 2. Results

### 118 2.1. Topography of Excited States

119 Thymine’s vertical excitation at ADC(2)/(aug-)cc-pVDZ level is characterized by a dark  $S_1$  state  
 120 at 4.56 eV with  $n\pi^*$  character and a bright  $S_2$  excitation at 5.06 eV with  $\pi\pi^*$  character (Table 2).  
 121 Electronic density differences for these two states in comparison to the ground state density are  
 122 shown in Figure 1.

123



124

125 **Figure 1.** (Left) Geometry of ground state thymine with atom numbering and main bond  
 126 lengths in Å. (Center) Difference between the electronic densities of the  $S_1$  state ( $n\pi^*$ ) and of the  
 127 ground state. (Right) Difference between the electronic densities of the  $S_2$  state ( $\pi\pi^*$ ) and of the  
 128 ground state. In this figure and throughout the paper, orange surfaces in the density difference  
 129 indicate electron deficient regions, while green surfaces indicate electron rich regions.

130 The main topographic points in these two excited states are the minima on  $S_2$  and  $S_1$ , the  
 131 intersection point between  $S_2$  and  $S_1$ , and the two intersection points between  $S_1$  and  $S_0$ . They are  
 132 characterized in Figure 2. Like in the Franck-Condon (FC) region, the  $S_2$  state around the  $S_2$  minimum  
 133 has a  $\pi\pi^*$  character. Nevertheless, while in the FC region the electron is promoted from a  $\pi$  bond  
 134 involving N1, C5, and C6, in the  $S_2$  minimum the electron is promoted from the C4O  $\pi$  bond (compare  
 135 the electronic density differences in Figure 1 and Figure 2). As a consequence of losing the C4O  $\pi$   
 136 bond in the  $S_2$  minimum, there is a strong stretching of the C4O distance from 1.23 Å in the FC region  
 137 to 1.48 Å in the  $S_2$  minimum. We will later discuss how this feature has a major impact on the  $S_2 \rightarrow S_1$   
 138 dynamics. Another feature of this minimum is a shrinking of the C4C5 and C5C6 bonds, indicating  
 139 the formation of  $\pi$  bonds in that region.

140 The  $S_1$  state in the  $S_1$  minimum still has the same  $n\pi^*$  character as in the FC region (electron  
 141 excitation from C4O). Compared to the ground state geometry, the main geometric consequence of  
 142 the relaxation into this minimum is the stretching of the C4O bond and the shrinking of the C4C5.

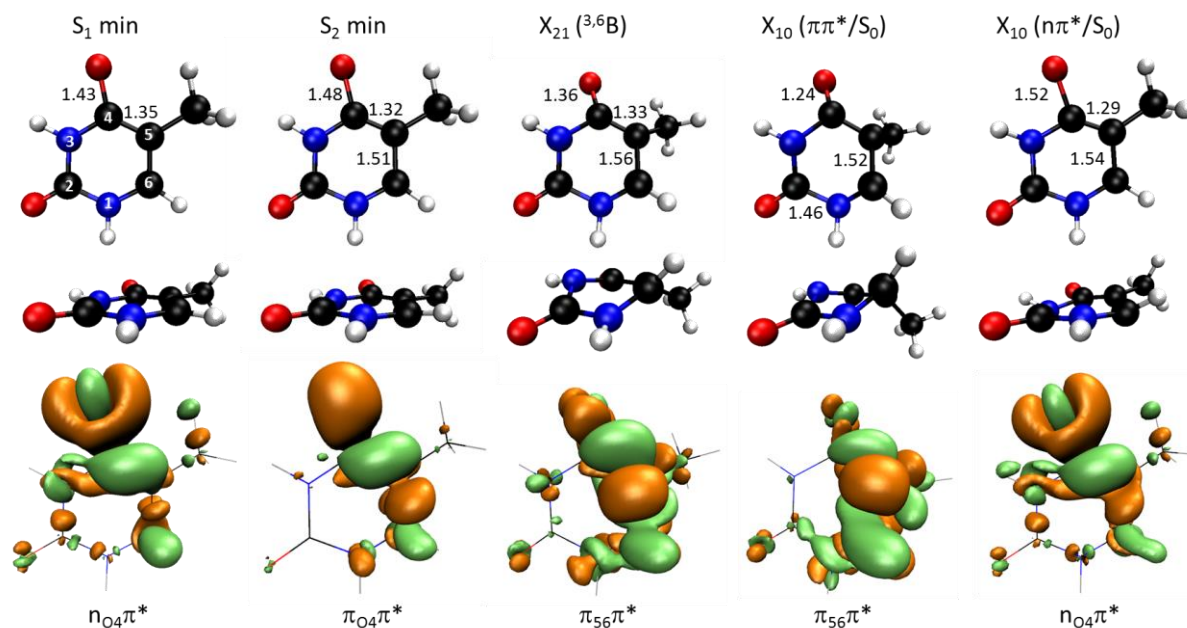
143 The crossing between  $S_2$  and  $S_1$  is reached by an out-of-plane deformation of the ring (Figure 2).  
 144 At the minimum energy crossing point, the ring assumes a boat conformation with N3 and C6 above  
 145 the plane ( ${}^3B$ ). Along the  $S_2$  state, this crossing still occurs on a  $\pi\pi^*$  state, but there is a significant  
 146 density change in comparison to that of the  $S_2$  minimum. While in the  $S_2$  minimum the C4O  $\pi$  bond  
 147 is lost, in the  $X_{21}$  crossing this bond it is formed back. This is clear from the shrinking of the C4O  
 148 distance from 1.48 to 1.36 Å between these two geometries. In fact, it is exactly this bond formation  
 149 responsible for the energy stabilization, which ultimately leads to the intersection.

150 The character change of the  $\pi\pi^*$  state between the FC region and the  $S_2$  minimum has been first  
 151 pointed out in ref. [21], while the character change between the  $S_2$  minimum and the  $X_{21}$  intersection  
 152 was first noticed in ref. [14]. Both works, however, were limited to an analysis of the main molecular  
 153 orbitals involved in the transitions. The density difference analysis goes a step further revealing more  
 154 precisely where the excitations are originated from.

155 **Table 2.** Ground and excited singlet state energies of the minima and intersection points of  
 156 thymine in the gas phase obtained with ADC(2), CASSCF, and MS-CASPT2. All energies are  
 157 relative to the ground state minimum.

Geometry	State	Energy (eV)		
		ADC(2)	CASSCF <sup>a</sup>	MS-CASPT2 <sup>b</sup>
$S_0$ min	$S_0$ (cs)	0.00	0.00	0.00
	$S_1$ ( $nO_4\pi^*$ )	4.56	5.19	5.09
	$S_2$ ( $\pi_{N1}\pi^*$ )	5.06	6.87	5.09
$S_1$ min	$S_0$ (cs)	1.33	1.39	1.02
	$S_1$ ( $nO_4\pi^*$ )	3.33	4.02	4.37
$S_2$ min	$S_0$ (cs)	2.14	1.71	1.28
	$S_1$ ( $nO_4\pi^*$ )	3.50	4.18	4.51
	$S_2$ ( $\pi_{O4}\pi^*$ )	4.18	5.64	4.77
$X_{10}$ ( $n\pi^*/S_0$ )	$S_0$ (cs)	3.90	5.02	5.02
	$S_1$ ( $nO_4\pi^*$ )	3.90	5.13	5.60
$X_{10}$ ( $\pi\pi^*/S_0$ )	$S_0$ (cs)	3.82	4.49	4.19
	$S_1$ ( $\pi_{56}\pi^*$ )	3.82	5.54	4.41
$X_{21}$ ( ${}^3B$ )	$S_0$ (cs)	3.37	2.68	2.23
	$S_1$ ( $nO_4\pi^*$ )	4.21	5.61	4.79
	$S_2$ ( $\pi_{56}\pi^*$ )	4.22	6.00	5.63

158 <sup>a</sup> CASSCF(12,9)/6-311G\* and <sup>b</sup> MS-CASPT2(12,9)/6-311G\* on CASSCF(8,6)/6-31G\* geometries; data from ref. [19].



159

160

161

162

163

**Figure 2.** Geometries of the  $S_1$  and  $S_2$  minima, and of the  $X_{21}$ ,  $X_{10} (\pi\pi^*/S_0)$  and  $X_{10} (n\pi^*/S_0)$  intersection points. The bond distances with the largest variation in comparison to the ground state geometry are given in Å. The electronic density difference between the relevant state in each case and the ground state are shown at the bottom.

164

165

166

167

168

169

170

There are two main minimum energy crossings between  $S_1$  and  $S_0$ . The first one connects the  $\pi\pi^*$  state to the ground state ( $X_{10} \pi_{56}\pi^*/S_0$  in Figure 2). It occurs as along the same type of geometrical distortion, giving rise to  $X_{21}$ . The  $X_{10} \pi\pi^*/S_0$  crossing also features a  ${}^3B$  boat conformation, but while the puckering degree is  $Q = 0.48$  Å for  $X_{21}$ , it increases further to  $Q = 0.54$  Å for  $X_{10}$  ( $Q$  is the Cremer-Pople parameter measuring the degree of puckering in a 6-membered ring [26]). At the crossing, the C4O  $\pi$  bond is fully formed and the C4O distance is 1.24 Å, essentially the same as in the ground state, 1.23 Å.

171

172

173

The second  $X_{10}$  crossing connects the  $n\pi^*$  state to the ground state ( $X_{10} n_{O4}\pi^*/S_0$  in Figure 2). It occurs as a further semi-planar distortion of the  $S_1$  minimum, with the C4O bond stretched to 1.52 Å and the C4C5 bond shrank to 1.29 Å.

174

175

176

177

This general topography of the lowest singlet excited states is illustrated in Figure 3. The top graph is the potential energy profile of the  $S_0$ ,  $S_1$ , and  $S_2$  states obtained by linear interpolation of internal coordinates (LIIC) between the two  $X_{10}$  intersection points. The bottom graph shows  $S_1$  and  $S_2$  along the interpolation between the  $S_2$  minimum and the  $X_{21}$  intersection.

178

179

180

181

182

183

As already mentioned, starting from the  $S_2$  minimum,  $X_{12}$  is reached by an out-of-plane distortion that recovers the C4O bond. With ADC(2), the cost for this bond formation is minimum, only 0.07 eV. For comparison, at CASSCF, the same interpolated barrier is 0.35 eV [14]. Note that these are linearly interpolated values, which overestimate the true barriers. Full optimization of transition states resulted in barriers of 0.25 eV with CASSCF [19] and between 0.01 and 0.05 eV with MS-CASPT2 [12,19].

184

185

186

187

188

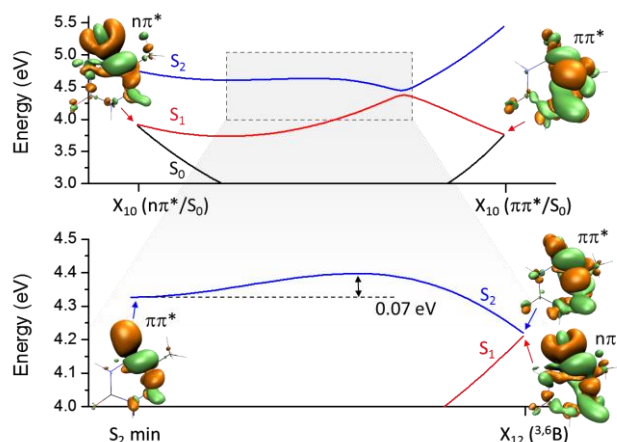
189

190

191

Although the qualitative description of the excited state topography of thymine obtained with ADC(2) is in agreement with previous description using other computational methods [1,15,19], it is clear from Table 2 that this agreement is merely qualitative. The quantitative description of the minima and intersection energies bears important differences between the methods. Unfortunately, at this point we cannot take for granted even that CASPT2 result would be the most accurate, as the usual protocol of computing CASPT2 energies on CASSCF optimized geometries may result in poor excitation energies, specially near the crossing seam (see, for instance, in Table 2, the large energy splits when MS-CASPT2 is used on CASSCF optimized intersection geometries). Having this

192 methodological warning in mind, we will present the dynamics results in the next section and later  
 193 discuss possible sources of inaccuracy on the ADC(2) surfaces.

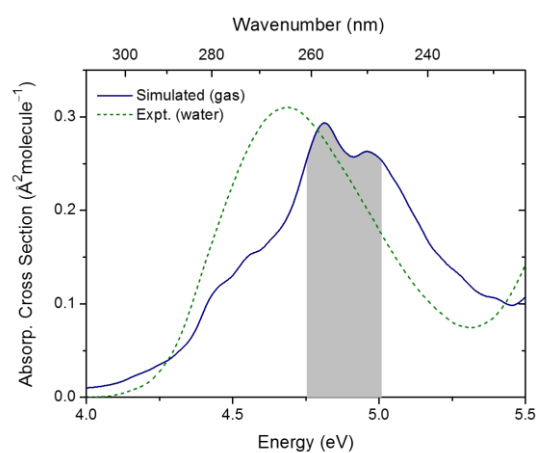


194

195 **Figure 3.** (Top) LIIC profile between the two  $X_{10}$  intersection points. (Bottom) LIIC profile  
 196 between the  $S_2$  minimum and the  $X_{21}$  intersection point. Electronic density differences at key  
 197 points are shown as well.

## 198 2.2. Dynamics

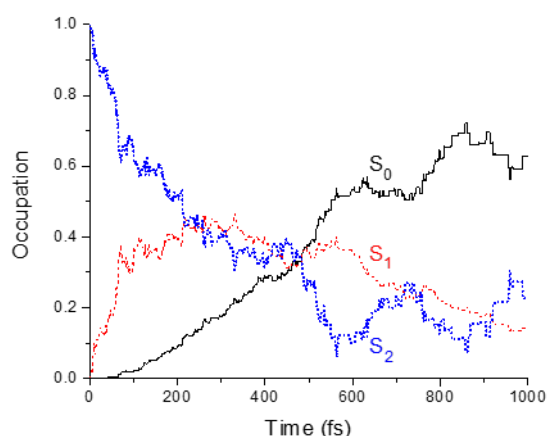
199 Initial conditions for dynamics were obtained by first simulating the absorption spectrum of  
 200 thymine in the gas phase. This spectrum is shown in Figure 4 compared to the experimental result in  
 201 water from ref. [27]. The ADC(2)/(aug)-cc-pVDZ absorption band is peaked at 4.89 eV. The  
 202 experimental gas phase result obtained by electron impact is  $4.95 \pm 0.08$  eV [28]. The absorption  
 203 intensity and band shape are also in very good agreement with the experimental results in water [27].



204

205 **Figure 4.** Simulated spectrum of thymine in the gas phase. The shaded area indicates where  
 206 initial conditions for dynamics were selected from. The dashed line is the experimental  
 207 spectrum of thymine in water from ref. [27].

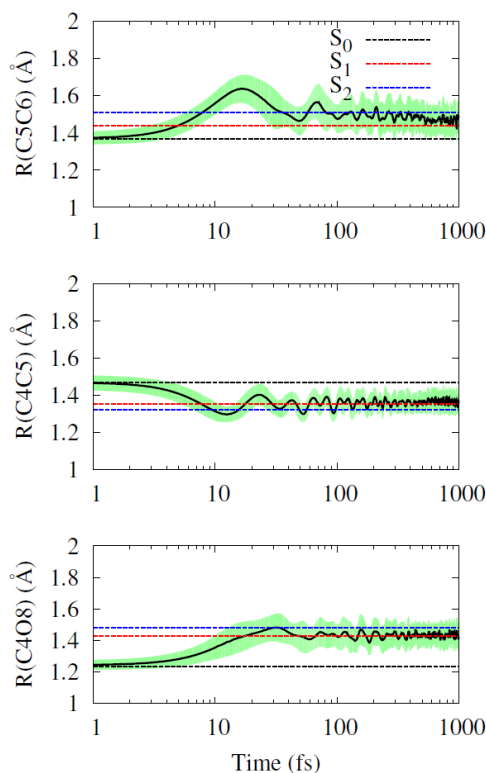
208 ADC(2)/(aug)-cc-pVDZ surface hopping dynamics of thymine in the gas phase shows a fast  
 209 relaxation process, with  $S_2$  converting to  $S_1$ , and then  $S_1$  converting to  $S_0$  (Figure 5). The fitting of the  
 210 state occupation (fraction of trajectories in each state) as a function of time shows a  $S_2 \rightarrow S_1$  exponential  
 211 decay of 84% of the population within 253 fs (Table 3). The fitting of the  $S_1$  occupation (see  
 212 Supplementary Material) reveals that 70% of the population returns to the ground state with 391 fs  
 213 time constant. A total of 30% of the population deactivates with time constant above 1 ps. Note that  
 214 considering a confidence level of 90%, our 115 trajectories only allow to tell these fractions within a  
 215 maximum statistical uncertainty of  $\pm 8\%$ .



216

217 **Figure 5.** State occupations during dynamics.

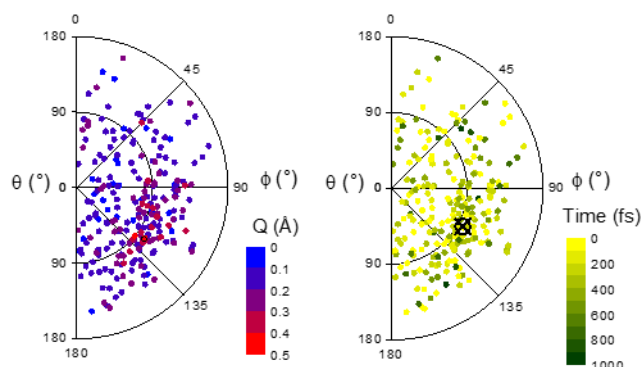
218 As we discussed in the previous section, the C5C6, C4C5, and C4O bond distances are markedly  
 219 distinct in the three state minima. Therefore, their evolution during the dynamics is useful to gather  
 220 further information on the state population. The time evolution of these bond distances averaged  
 221 over all trajectories are shown in Figure 6. All three start near the optimal  $S_0$  minimum value. The  $S_2$   
 222 minimum is quickly reached, after 100 fs. This can be clearly seen only in the C5C6 bond, which bears  
 223 the largest difference between  $S_1$  and  $S_2$  minima. In the other two cases, the large number of  
 224 trajectories quickly decaying to  $S_1$  together with the large standard deviation tend to hide this feature.  
 225 By the end of the simulations, the three bond distances oscillate near the  $S_1$  minimum. (As we discuss  
 226 in the Theoretical and Computational Details, we do not simulate the ground state dynamics. For this  
 227 reason, in the long term, we do not see the ground state bond distances being recovered.)



228

229 **Figure 6.** Time evolution of the C5C6, C4C5, and C4O bond distances averaged over all  
 230 trajectories. The shaded areas show +/- one standard deviation around the mean value.  
 231 Horizontal lines indicate the optimal values of the  $S_0$ ,  $S_1$  and  $S_2$  minima.

232



233

234

235

236

237

**Figure 7.** Polar plot showing the distribution of Cremer-Pople parameters  $\theta$  and  $\phi$  at the  $S_2/S_1$  hop geometry. At left, the colors additionally indicate the value of the third parameter  $Q$ . At right, the color code indicates the hop time. Both maps were symmetry-projected to show only  $\phi < 180^\circ$  region. The crossed circle indicates the minimum energy crossing point.

238

239

240

241

242

243

The  $S_2 \rightarrow S_1$  conversion occurs in a wide variety of ring puckering conformations, including distortions far away from the minimum intersection point. This is illustrated in Figure 7, which shows the distribution of Cremer-Pople parameters  $\theta$  and  $\phi$  at the  $S_2/S_1$  hop point. (These two parameters characterize the type of puckering in a 6-membered ring.) Larger ring distortions (large  $Q$ ) tend to occur near the  ${}^3,6B$  region ( $\theta = 90^\circ$ ,  $\phi = 120^\circ$ ). There is no correlation between the type of ring puckering and the hop time.

244

245

246

The  $S_1 \rightarrow S_0$  conversion occurs at both branches of intersection, the  $n\pi^*/S_0$  and the  $\pi\pi^*/S_0$ . From the 84% of the population converting to  $S_1$ , 61% deactivates in the  $n\pi^*/S_0$  crossing and 9% in the  $\pi\pi^*/S_0$ . Finally, 14% of the population does not decay in the sub-picosecond process and remains in  $S_1$ .

247

248

249

250

**Table 3.** Time constants for different processes and corresponding fractions of population being affected by them. For  $S_2 \rightarrow S_1$  and  $S_1 \rightarrow S_0$  processes, parameters were obtained by fitting the state occupations in Figure 5 with the kinetic model discussed in the Supplementary Material. For  $FC \rightarrow S_2$  min, the information was extracted from Figure 6.

Process	$f_\tau$	$\tau$ (fs)
$FC \rightarrow S_2$ min	1.00	~100
$S_2 \rightarrow S_1$	0.84	253
$S_1 \rightarrow S_0$	0.70	391

251

### 3. Discussion

252

253

254

255

256

257

258

259

The results of the ADC(2) surface hopping dynamics of thymine in the gas phase are schematically summarized in Figure 8. After photoexcitation into the  $\pi_{N1}\pi^*$  state (a), thymine relaxes within 100 fs to the minimum of the  $S_2$  surface holding a  $\pi_{O4}\pi^*$  character (b). A minor fraction of the population is trapped in  $S_2$  (c), while the remaining flows to  $S_1$  in about 250 fs (d). This conversion to  $S_1$  splits the population once more: a minor part follows the  $S_1$  state along the  $\pi_{56}\pi^*$  branch and immediately converts to the ground state (e); the major part, however, flows to the  $S_1$   $n_{O4}\pi^*$  minimum (f). After about 400 fs, most of population converts to the ground state in the  $n_{O4}\pi^*/S_0$  crossing (g), while a minor fraction remains trapped in the  $S_1$  state (h).

260

261

262

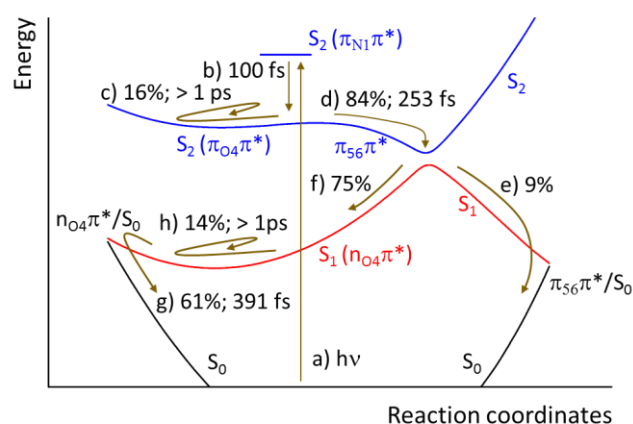
263

264

265

These results imply that, upon inclusion of electron dynamic correlation in the dynamics, the  $S_2$  trapping is drastically reduced and may affect only 16% of the population. In CASSCF dynamics, it affects about 80% of the population [14]. This difference is a strong indication that dynamics based on CASSCF [14,23] may have overestimated the role of the  $S_2$  trapping. And the reason for this overestimation is clear: in CASSCF the formation of C4O  $\pi$  bond (which allows to reach the  $S_2/S_1$  intersection) has an energetic cost, in the form of a barrier (0.25 eV [19]) separating the  $S_2$  minimum

266 and the intersection. This barrier practically disappears when dynamic electron correlation is  
 267 included, either in ADC(2) or in CASPT2.  
 268



269

270 **Figure 8.** Schematic view of thymine dynamics as predicted by ADC(2) surface hopping. See  
 271 text for description.

272 ADC(2) is a single reference method, whose current implementation is based on linear response  
 273 theory. Naturally, we cannot expect that it will provide definitive answers on thymine time constants.  
 274 Moreover, we should consider that we cannot accurately compute the time constant for deactivation  
 275 to  $S_0$  due to the lack of  $S_1/S_0$  nonadiabatic couplings. As explained later in the section Theoretical and  
 276 Experimental Details, we deal with this problem using an energy threshold as hop criterion. For this  
 277 reason, both  $S_1 \rightarrow S_0$  time constant and fraction of population bear large uncertainties. For instance, if  
 278 we double the energy gap threshold from 0.15 to 0.30 eV, the  $S_1 \rightarrow S_0$  time constant is reduced from  
 279 391 to 291 fs.

280 In particular, the efficient  $S_1/S_0$  conversion of 70% of the population in the sub-picosecond scale  
 281 is specially challenging to be rationalized in view of the experimental signal in the few picoseconds  
 282 range (Table 1). Even if the third of the population which is left in the excited states decayed with a  
 283 time constant spanning few picoseconds, this fraction may be too small to account for the strong ion  
 284 signal originating from this spectral region. Nevertheless, without a full spectral simulation including  
 285 the probe process, we also cannot discard the possibility that this third of the population is in fact  
 286 ultimately responsible for the signal. (Unfortunately, the experimental references do not disclose the  
 287 fitting amplitudes in addition to the time constants. They would be invaluable to check this point.)

288 If the fraction of the population decaying in the picosecond scale is significantly larger than 30%,  
 289 this will indicate that the  $n\pi^*/S_0$  intersection predicted by ADC(2) is too low in energy, which could  
 290 be result of the wrong topography of the  $S_1/S_0$  crossing seam at this level [29]. However, even if we  
 291 come to conclude that ADC(2) dynamics is artificially fast, it seems improbable that its prediction of  
 292 sub-picosecond  $S_1/S_0$  conversion is completely wrong. The occurrence of this fast process in thymine  
 293 should be seriously considered, as it has recurrently shown up in the simulations: it is relevant in  
 294 ADC(2) dynamics, dominant in semi-empirical OM2/MRCI dynamics [20], and even in CASSCF  
 295 dynamics it affects about 20% of the population [14]. In practical terms, it means that the current trend  
 296 of fitting time-resolved spectra of thymine with three exponential decays with fs, ps, and ns time  
 297 constants may be too strict. We may even recall alternative fittings, like that in ref. [3], which split the  
 298 sub-picosecond time constant in two, <50 fs and 490 fs.

299 Photodynamics of thymine has daring experimentalists and theoreticians. Although we are still  
 300 not in position of delivering a final assignment of its many spectral features, it is becoming obvious  
 301 that assigning its time constants to single processes may be the wrong strategy. The ensemble of  
 302 results points out to a situation where several processes contribute to the dynamics in the same time  
 303 scale. In particular, it is astonishing that in the sub-picosecond time scale alone, the time resolved

304 spectra may be influenced by laser field, variation of the IP along S<sub>2</sub> relaxation through three different  
305 ππ\* characters, S<sub>2</sub>/S<sub>1</sub> conversion, and S<sub>1</sub>/S<sub>0</sub> conversion in two different branches of the crossing seam.  
306 To learn how to resolve each of them is the next challenge.

## 307 4. Theoretical and Computational Details

### 308 4.1 Potential energy, spectrum, and dynamics simulations

309 The geometries of the ground and the first two singlet excited states of thymine were optimized  
310 with algebraic diagrammatic construction to second order (ADC(2)) level [30,31] (for the ground  
311 state, on MP2 level). The Dunning's aug-cc-pVDZ basis set was used for all elements except for  
312 hydrogen, where cc-pVDZ was employed [32]. This mixed basis set is denoted (aug-)cc-pVDZ in the  
313 text. Calculations were done with frozen core and applying the resolution-of-identity (RI)  
314 approximation for the computation of two-electron integrals. In addition to state minima, we also  
315 optimized two intersection minima between S<sub>0</sub> and S<sub>1</sub> states (denoted X<sub>10</sub>), and an intersection  
316 minimum between S<sub>2</sub> and S<sub>1</sub> (denoted as X<sub>21</sub>). Reaction paths were computed applying linear  
317 interpolation in natural internal coordinates (LIIC) [33].

318 We simulated the photoabsorption spectrum of thymine applying the nuclear ensemble  
319 approach [34]. A set of 500 molecular geometries and momenta was created using harmonic-oscillator  
320 Wigner distribution, on the basis of normal modes in the ground state. Vertical excitation energies  
321 and oscillator strengths for transitions to the first ten singlet states were computed using  
322 ADC(2)/(aug-)cc-pVDZ for each geometry in the ensemble.

323 We performed nonadiabatic excited-state dynamics simulations using surface hopping on  
324 ADC(2)/(aug-)cc-pVDZ potential energy surfaces. The initial conditions (geometries and momenta)  
325 for dynamics simulations were selected starting from the bright S<sub>2</sub> state. They were filtered from the  
326 initial ensemble of 500 initial conditions, from within the 4.88 ± 0.13 eV energy window, which  
327 includes the maximum of the first band in the spectrum. This procedure produced 115 initial  
328 conditions, which were propagated for a maximum 1 ps.

329 Nonadiabatic events between S<sub>2</sub> and S<sub>1</sub> were taken into account by the fewest switches algorithm  
330 [35] corrected for decoherence effects (α = 0.1 Hartree) [36]. Because of the limitation of ADC(2) to  
331 deal with multi-reference ground states [29], trajectories were stopped whenever their S<sub>1</sub>/S<sub>0</sub> energy  
332 gap dropped below 0.15 eV. The corresponding time step was taken as an estimate of the S<sub>1</sub>/S<sub>0</sub>  
333 crossing time. The Newton's equations of motion were integrated using velocity Verlet algorithm [37]  
334 with the time step of 0.5 fs. Integration of the semi-classical Schrödinger equation was done  
335 employing the 5th order Butcher's algorithm [38] with time step of 0.025 fs, using interpolated  
336 electronic properties between the classical steps. Computation of nonadiabatic couplings between  
337 excited states is described in the next section.

338 To analyze the distortions of thymine's ring during dynamics, we computed the Cremer-Pople  
339 parameters [26] and classified them into conformations according to Boeyens' scheme [39].

340 All ADC(2) computations were done with TURBOMOLE [40]. Spectrum and dynamics were  
341 computed with the NEWTON-X / TURBOMOLE interface [41,42]. Intersection point optimizations  
342 were done with an in-house modified version of CIOpt program [43]. Cremer-Pople parameters were  
343 obtained using the PLATON program [44].

### 344 4.2 OD method for coupling calculations

345 Nonadiabatic couplings  $\sigma_{mn}$  between electronic states  $m$  and  $n$  can be dynamically estimated on  
346 the basis of the time derivative of the corresponding wave functions during the trajectory:

$$347 \sigma_{mn} = \langle \Psi_m | \partial_t \Psi_n \rangle. \quad (1)$$

348 When computed by finite differences, time-derivative nonadiabatic couplings (TDNC)  $\sigma_{mn}$  can be  
349 conveniently written in terms of wave function overlaps between consecutive time steps. Then, as  
350 proposed by Hammes-Schiffer and Tully [45], TDNC can be used to evaluate the fewest-switches  
351 probability formula, by directly replacing the inner product between the nonadiabatic coupling

352 vector and the nuclear velocities,  $\sigma_{mn} = \mathbf{F}_{mn} \cdot \mathbf{v}$ . This procedure has become popular, as it allows to  
 353 overcome the cumbersome evaluation of nonadiabatic coupling vectors [46-48].

354 In the present work, TDNC are obtained by evaluating eq. (1) with the OD (for *orbital derivatives*)  
 355 method proposed in ref. [49]. This method requires computation of time derivatives (and wave  
 356 function overlaps) on a basis of molecular orbitals, rather than on a basis of Slater determinants as  
 357 usually done. (This latter approach will be referred as DD, for *determinant derivative*, method.)

358 The OD method is discussed in detail in ref. [49]. Here, we briefly outline the main points to  
 359 explain its current implementation in NEWTON-X. Considering a configuration interaction  
 360 expansion of singly excited determinants (CIS)  $|\Phi_i^a\rangle = \hat{a}_a^\dagger \hat{a}_i |\Phi_0\rangle$ , the electronic wave function for  
 361 state  $m$  is

$$362 \quad |\Psi_m\rangle = \sum_{ia} C_{ia}^m |\Phi_i^a\rangle. \quad (2)$$

363 The couplings between the excited states  $m$  and  $n$  can be evaluated as

$$364 \quad \sigma_{mn} = \sum_{ia} C_{ia}^m \partial_t C_{ia}^n + \sum_{iab} C_{ia}^m C_{jb}^n \langle \varphi_a | \partial_t \varphi_b \rangle - \sum_{ija} P_{ij} C_{ia}^m C_{jb}^n \langle \varphi_j | \partial_t \varphi_i \rangle, \quad (3)$$

365 where  $P_{ij}$  is a phase that depends on the ordering convention adopted for the molecular orbitals  
 366  $\{\varphi_k\}$  in the Slater determinants.

367 Considering the overlap matrix between molecular orbitals from two consecutive times steps,  
 368 the time derivatives of the molecular orbitals are evaluated by finite differences:

$$369 \quad \langle \varphi_j | \partial_t \varphi_i \rangle \approx \frac{\langle \varphi_j(t) | \varphi_i(t + \Delta t) \rangle}{\Delta t} \equiv \frac{S_{ji}(t, t + \Delta t)}{\Delta t}, \quad (4)$$

370 where  $S_{ji}$  is the orbital overlap matrix. An orbital phase matching algorithm is used to assure the  
 371 continuity of orbitals at different time steps.

372 The formal scaling of the TDNC evaluation is reduced from  $N_{occ}^5 N_{virt}^2$  in the DD approach to  
 373  $N_{occ} N_{virt}^2$  in the OD. This method has shown excellent results in comparison to the DD at significantly  
 374 lower computational costs [49]. In the present simulations of thymine, for instance, computation of  
 375 TDNC with the OD method was ten times faster than with the DD method.

376 We have implemented the OD method in NEWTON-X, where it is available for GAUSSIAN [50]  
 377 (CIS, TDA, and TDDFT methods) and TURBOMOLE (TDA, TDDFT, CC2, and ADC(2) methods)  
 378 interfaces. In particular, for the density functional based methods, approximated CIS wave functions  
 379 are built using the Casida Ansatz [51,52]. In the case of ADC(2) and CC2, approximated CIS wave  
 380 functions are expressed in terms of Jacobian eigenvectors, where double excitations are neglected and  
 381 the resulting wave functions are reorthonormalized [53].

382 **Supplementary Materials:** The following are available online at [www.mdpi.com/link](http://www.mdpi.com/link), kinetic model to fit  
 383 occupations and Cartesian coordinates for all structures.

384 **Acknowledgments:** L.S., S.B., and M.B. thank the support of the A\*MIDEX grant (n° ANR-11-IDEX-0001-02)  
 385 funded by the French Government « Investissements d’Avenir » program supervised by the Agence Nationale  
 386 de la Recherche. This work was granted access to the HPC resources of Aix-Marseille Université financed by the  
 387 project Equip@Meso (ANR-10-EQPX-29-01) also within the « Investissements d’Avenir » program. A.F.I.  
 388 acknowledges funding from a Sloan Research Fellowship and the Natural Sciences and Engineering Research  
 389 Council of Canada (NSERC) through the Discovery Grants Program.

390 **Author Contributions:** M.B. and H.L. conceived and designed the simulations; L.S. and S.B. performed the  
 391 simulations; J.N., R.C., and A.F.I. developed and implemented the coupling method; L.S., R.C., and M.B. wrote  
 392 the paper.

393 **Conflicts of Interest:** The authors declare no conflict of interest. The founding sponsors had no role in the design  
 394 of the study; in the collection, analyses, or interpretation of data; in the writing of the manuscript, and in the  
 395 decision to publish the results.

396 **References**

- 397 1. Yu, H.; Sanchez-Rodriguez, J.A.; Pollum, M.; Crespo-Hernandez, C.E.; Mai, S.; Marquetand, P.;  
398 Gonzalez, L.; Ullrich, S. Internal conversion and intersystem crossing pathways in uv excited, isolated  
399 uracils and their implications in prebiotic chemistry. *Phys. Chem. Chem. Phys.* **2016**, *18*, 20168-20176.
- 400 2. Kang, H.; Lee, K.T.; Jung, B.; Ko, Y.J.; Kim, S.K. Intrinsic lifetimes of the excited state of DNA and rna  
401 bases. *J. Am. Chem. Soc.* **2002**, *124*, 12958-12959.
- 402 3. Ullrich, S.; Schultz, T.; Zgierski, M.Z.; Stolow, A. Electronic relaxation dynamics in DNA and rna bases  
403 studied by time-resolved photoelectron spectroscopy. *Phys. Chem. Chem. Phys.* **2004**, *6*, 2796-2801.
- 404 4. McFarland, B.K.; Farrell, J.P.; Miyabe, S.; Tarantelli, F.; Aguilar, A.; Berrah, N.; Bostedt, C.; Bozek, J.D.;  
405 Bucksbaum, P.H.; Castagna, J.C., *et al.* Ultrafast x-ray auger probing of photoexcited molecular  
406 dynamics. *Nat Commun* **2014**, *5*, 4235.
- 407 5. Gonzalez-Vazquez, J.; Gonzalez, L.; Samoylova, E.; Schultz, T. Thymine relaxation after uv irradiation:  
408 The role of tautomerization and  $\pi\sigma^*$  states. *Phys. Chem. Chem. Phys.* **2009**, *11*, 3927-3934.
- 409 6. Gador, N.; Samoylova, E.; Smith, V.R.; Stolow, A.; Rayner, D.M.; Radloff, W.; Hertel, I.V.; Schultz, T.  
410 Electronic structure of adenine and thymine base pairs studied by femtosecond electron-ion  
411 coincidence spectroscopy. *J. Phys. Chem. A* **2007**, *111*, 11743-11749.
- 412 7. Canuel, C.; Mons, M.; Piuze, F.; Tardivel, B.; Dimicoli, I.; Elhanine, M. Excited states dynamics of DNA  
413 and rna bases: Characterization of a stepwise deactivation pathway in the gas phase. *J. Chem. Phys.*  
414 **2005**, *122*, 074316-074316.
- 415 8. Samoylova, E.; Schultz, T.; Hertel, I.V.; Radloff, W. Analysis of ultrafast relaxation in photoexcited DNA  
416 base pairs of adenine and thymine. *Chem. Phys.* **2008**, *347*, 376-382.
- 417 9. Ligare, M.; Siouri, F.; Bludsky, O.; Nachtigalova, D.; de Vries, M.S. Characterizing the dark state in  
418 thymine and uracil by double resonant spectroscopy and quantum computation. *Phys. Chem. Chem.*  
419 *Phys.* **2015**, *17*, 24336-24341.
- 420 10. Samoylova, E.; Lippert, H.; Ullrich, S.; Hertel, I.V.; Radloff, W.; Schultz, T. Dynamics of photoinduced  
421 processes in adenine and thymine base pairs. *J. Am. Chem. Soc.* **2005**, *127*, 1782-1786.
- 422 11. Barbatti, M.; Borin, A.; Ullrich, S. Photoinduced processes in nucleic acids. In *Photoinduced phenomena*  
423 *in nucleic acids*; Barbatti, M.; Borin, A.C.; Ullrich, S., Eds. Springer International Publishing: 2015; Vol.  
424 355, pp 1-32.
- 425 12. Yamazaki, S.; Taketsugu, T. Nonradiative deactivation mechanisms of uracil, thymine, and 5-  
426 fluorouracil: A comparative ab initio study. *J. Phys. Chem. A* **2012**, *116*, 491-503.
- 427 13. Perun, S.; Sobolewski, A.L.; Domcke, W. Conical intersections in thymine. *J. Phys. Chem. A* **2006**, *110*,  
428 13238-13244.
- 429 14. Szymczak, J.J.; Barbatti, M.; Soo Hoo, J.T.; Adkins, J.A.; Windus, T.L.; Nachtigallová, D.; Lischka, H.  
430 Photodynamics simulations of thymine: Relaxation into the first excited singlet state. *J. Phys. Chem. A*  
431 **2009**, *113*, 12686-12693.
- 432 15. Zechmann, G.; Barbatti, M. Photophysics and deactivation pathways of thymine. *J. Phys. Chem. A* **2008**,  
433 *112*, 8273-8279.
- 434 16. Serrano-Pérez, J.J.; González-Luque, R.; Merchán, M.; Serrano-Andrés, L. On the intrinsic population  
435 of the lowest triplet state of thymine. *J. Phys. Chem. B* **2007**, *111*, 11880-11883.
- 436 17. Bai, S.; Barbatti, M. Why replacing different oxygens of thymine with sulfur causes distinct absorption  
437 and intersystem crossing. *J. Phys. Chem. A* **2016**, DOI:10.1021/acs.jpca.1026b05110.

- 438 18. Merchán, M.; González-Luque, R.; Climent, T.; Serrano-Andrés, L.; Rodriiguez, E.; Reguero, M.; Pelaez,  
439 D. Unified model for the ultrafast decay of pyrimidine nucleobases. *J. Phys. Chem. B* **2006**, *110*, 26471-  
440 26476.
- 441 19. Asturiol, D.; Lasorne, B.; Robb, M.A.; Blancafort, L. Photophysics of the  $\pi,\pi^*$  and  $n,\pi^*$  states of thymine:  
442 Ms-caspt2 minimum-energy paths and casscf on-the-fly dynamics. *J. Phys. Chem. A* **2009**, *113*, 10211-  
443 10218.
- 444 20. Lan, Z.; Fabiano, E.; Thiel, W. Photoinduced nonadiabatic dynamics of pyrimidine nucleobases: On-  
445 the-fly surface-hopping study with semiempirical methods. *J. Phys. Chem. B* **2009**, *113*, 3548-3555.
- 446 21. González, L.; González-Vázquez, J.; Samoylova, E.; Schultz, T. On the puzzling deactivation mechanism  
447 of thymine after light irradiation. *AIP Conf. Proc.* **2008**, *1080*, 169-175.
- 448 22. Arbelo-González, W.; Crespo-Otero, R.; Barbatti, M. Steady and time-resolved photoelectron spectra  
449 based on nuclear ensembles. *J. Chem. Theory Comput.* **2016**, doi:10.1021/acs.jctc.1026b00704.
- 450 23. Hudock, H.R.; Levine, B.G.; Thompson, A.L.; Satzger, H.; Townsend, D.; Gador, N.; Ullrich, S.; Stolow,  
451 A.; Martínez, T.J. Ab initio molecular dynamics and time-resolved photoelectron spectroscopy of  
452 electronically excited uracil and thymine. *J. Phys. Chem. A* **2007**, *111*, 8500-8508.
- 453 24. Barbatti, M.; Aquino, A.J.A.; Szymczak, J.J.; Nachtigallová, D.; Hobza, P.; Lischka, H. Relaxation  
454 mechanisms of uv-photoexcited DNA and rna nucleobases. *Proc. Natl. Acad. Sci. USA* **2010**, *107*, 21453-  
455 21458.
- 456 25. Picconi, D.; Barone, V.; Lami, A.; Santoro, F.; Improta, R. The interplay between  $\pi\pi^*/n\pi^*$  excited states  
457 in gas-phase thymine: A quantum dynamical study. *ChemPhysChem* **2011**, *12*, 1957-1968.
- 458 26. Cremer, D.; Pople, J.A. General definition of ring puckering coordinates. *J. Am. Chem. Soc.* **1975**, *97*,  
459 1354-1358.
- 460 27. Zhu, X.-M.; Wang, H.-g.; Zheng, X.; Phillips, D.L. Role of ribose in the initial excited state structural  
461 dynamics of thymidine in water solution: A resonance raman and density functional theory  
462 investigation. *J. Phys. Chem. B* **2008**, *112*, 15828-15836.
- 463 28. Abouaf, R.; Pommier, J.; Dunet, H. Electronic and vibrational excitation in gas phase thymine and 5-  
464 bromouracil by electron impact. *Chem. Phys. Lett.* **2003**, *381*, 486-494.
- 465 29. Tuna, D.; Lefrancois, D.; Wolański, Ł.; Gozem, S.; Schapiro, I.; Andruniów, T.; Dreuw, A.; Olivucci, M.  
466 Assessment of approximate coupled-cluster and algebraic-diagrammatic-construction methods for  
467 ground- and excited-state reaction paths and the conical-intersection seam of a retinal-chromophore  
468 model. *J. Chem. Theory Comput.* **2015**, *11*, 5758-5781.
- 469 30. Trofimov, A.B.; Schirmer, J. An efficient polarization propagator approach to valence electron excitation  
470 spectra. *J. Phys. B: At., Mol. Opt. Phys.* **1995**, *28*, 2299-2324.
- 471 31. Schirmer, J. Beyond the random-phase approximation: A new approximation scheme for the  
472 polarization propagator. *Phys. Rev. A* **1982**, *26*, 2395-2416.
- 473 32. Dunning Jr., T.H. Gaussian basis sets for use in correlated molecular calculations. I. The atoms boron  
474 through neon and hydrogen. *J. Chem. Phys.* **1989**, *90*, 1007-1023.
- 475 33. Fogarasi, G.; Zhou, X.F.; Taylor, P.W.; Pulay, P. The calculation of abinitio molecular geometries -  
476 efficient optimization by natural internal coordinates and empirical correction by offset forces. *J. Am.*  
477 *Chem. Soc.* **1992**, *114*, 8191-8201.
- 478 34. Crespo-Otero, R.; Barbatti, M. Spectrum simulation and decomposition with nuclear ensemble: Formal  
479 derivation and application to benzene, furan and 2-phenylfuran. *Theor. Chem. Acc.* **2012**, *131*, 1237.
- 480 35. Tully, J.C. Molecular-dynamics with electronic-transitions. *J. Chem. Phys.* **1990**, *93*, 1061-1071.

- 481 36. Granucci, G.; Persico, M. Critical appraisal of the fewest switches algorithm for surface hopping. *J.*  
482 *Chem. Phys.* **2007**, *126*, 134114-134111.
- 483 37. Swope, W.C.; Andersen, H.C.; Berens, P.H.; Wilson, K.R. A computer-simulation method for the  
484 calculation of equilibrium-constants for the formation of physical clusters of molecules - application to  
485 small water clusters. *J. Chem. Phys.* **1982**, *76*, 637-649.
- 486 38. Butcher, J. A modified multistep method for the numerical integration of ordinary differential  
487 equations. *J. Assoc. Comp. Mach.* **1965**, *12*, 124-135.
- 488 39. Boeyens, J.C.A. The conformation of six-membered rings. *J. Chem. Crystallogr.* **1978**, *8*, 317-320.
- 489 40. Ahlrichs, R.; Bär, M.; Häser, M.; Horn, H.; Kölmel, C. Electronic-structure calculations on workstation  
490 computers - the program system turbomole. *Chem. Phys. Lett.* **1989**, *162*, 165-169.
- 491 41. Barbatti, M.; Ruckebauer, M.; Plasser, F.; Pittner, J.; Granucci, G.; Persico, M.; Lischka, H. Newton-x:  
492 A surface-hopping program for nonadiabatic molecular dynamics. *WIREs: Comp. Mol. Sci.* **2014**, *4*, 26-  
493 33.
- 494 42. Barbatti, M.; Granucci, G.; Ruckebauer, M.; Plasser, F.; Crespo-Otero, R.; Pittner, J.; Persico, M.;  
495 Lischka, H. *Newton-x: A package for newtonian dynamics close to the crossing seam*. [www.newtonx.org](http://www.newtonx.org)  
496 (accessed september 1, 2016). 2013.
- 497 43. Levine, B.G.; Coe, J.D.; Martínez, T.J. Optimizing conical intersections without derivative coupling  
498 vectors: Application to multistate multireference second-order perturbation theory (ms-caspt2). *J. Phys.*  
499 *Chem. B* **2008**, *112*, 405-413.
- 500 44. Spek, A.L. Single-crystal structure validation with the program platon. *J. Appl. Crystallogr.* **2003**, *36*, 7-  
501 13.
- 502 45. Hammes-Schiffer, S.; Tully, J.C. Proton-transfer in solution - molecular-dynamics with quantum  
503 transitions. *J. Chem. Phys.* **1994**, *101*, 4657-4667.
- 504 46. Pittner, J.; Lischka, H.; Barbatti, M. Optimization of mixed quantum-classical dynamics: Time-  
505 derivative coupling terms and selected couplings. *Chem. Phys.* **2009**, *356*, 147-152.
- 506 47. Werner, U.; Mitrić, R.; Suzuki, T.; Bonačić-Koutecký, V. Nonadiabatic dynamics within the time  
507 dependent density functional theory: Ultrafast photodynamics in pyrazine. *Chem. Phys.* **2008**, *349*, 319-  
508 324.
- 509 48. Tapavicza, E.; Tavernelli, I.; Rothlisberger, U. Trajectory surface hopping within linear response time-  
510 dependent density-functional theory. *Phys. Rev. Lett.* **2007**, *98*, 023001-023004.
- 511 49. Ryabinkin, I.G.; Nagesh, J.; Izmaylov, A.F. Fast numerical evaluation of time-derivative nonadiabatic  
512 couplings for mixed quantum-classical methods. *J. Phys. Chem. Lett.* **2015**, *6*, 4200-4203.
- 513 50. Frisch, M.J.; Trucks, G.W.; Schlegel, H.B.; Scuseria, G.E.; Robb, M.A.; Cheeseman, J.R.; Scalmani, G.;  
514 Barone, V.; Mennucci, B.; Petersson, G.A., et al. *Gaussian 09, Revision D.01*. Gaussian, Inc., Wallingford CT  
515 **2013**.
- 516 51. Casida, M. Time-dependent density functional response theory for molecules. In *Recent advances in*  
517 *density functional methods, part i*, Chong, D., Ed. World Scientific: Singapore, 1995; pp 155-192.
- 518 52. Barbatti, M.; Crespo-Otero, R. Surface hopping dynamics with dft excited states. In *Density-functional*  
519 *methods for excited states*, Ferré, N.; Filatov, M.; Huix-Rotllant, M., Eds. Springer International  
520 Publishing: Cham, 2016; pp 415-444.
- 521 53. Plasser, F.; Crespo-Otero, R.; Pederzoli, M.; Pittner, J.; Lischka, H.; Barbatti, M. Surface hopping  
522 dynamics with correlated single-reference methods: 9h-adenine as a case study. *J. Chem. Theory Comput.*  
523 **2014**, *10*, 1395-1405.
- 524

525 © 2016 by the authors. Submitted for possible open access publication under the  
 terms and conditions of the Creative Commons Attribution (CC-BY) license  
(<http://creativecommons.org/licenses/by/4.0/>).

528